*Paper accepted for publication by Journal of Rail and Rapid Transit, 15 April 2017*

# Estimation of track parameters and wheel–rail combined roughness from rail vibration

Qi Li[1], David J Thompson[2], Martin G R Toward[2]

[1]Department of Bridge Engineering, Tongji University, 1239 Siping Road, Shanghai 200092, China.
[2] Institute of Sound and Vibration Research, University of Southampton, Southampton SO17 1BJ, UK.
Corresponding author:

Qi Li, Department of Bridge Engineering, Tongji University,1239 Siping Road, Shanghai 200092, China.
Email: liqi_bridge@tongji.edu.cn

## Abstract

Rolling noise from railways is significantly affected by the wheel–rail combined roughness and the dynamic properties of the track. To facilitate vibration and noise predictions it is desirable to be able to determine these parameters accurately from field measurements. In this study an inverse method to determine these parameters is adopted and enhanced. Use is made of a track model based on a wavenumber finite element model of the free rail coupled to discrete supports, which allows for the pinned–pinned mode and cross–sectional deformation of the rail. The rail vibration induced by hammer impacts and the vibration during train passages are simulated using this model, and these results are then applied to illustrate the accuracy of the direct and indirect methods for the estimation of track decay rate. These methods are compared in a case study for a ballasted track for which hammer impact and train pass-by measurements have been obtained. Other track parameters can also be extracted from the measured data by using the advanced track model. Thereafter a more complete method is adopted to estimate the wheel–rail combined roughness from measured rail vibration under train passages. A comparison is conducted among the estimated roughness levels obtained from this full method, an existing simplified method and the direct measurement method. It is found that the simplified method overestimates the roughness around the pinned–pinned resonance frequency but gives a good estimation if the track decay

rates of the loaded track are used.

**Keywords**

ballasted track, wheel–rail interaction, track decay rate, roughness, parameter estimation

## Introduction

Noise from railway traffic has gained increasing attention since the 1960s with the rapid development of rail networks worldwide and growing awareness of the adverse effects of noise on human health and well–being[1]. Many studies have been conducted to understand the generation and propagation of rolling noise from railways[2-5]. The rail and wheel vibration are the most important sources[1] of rolling noise from straight railway lines operating at normal speeds. The critical parameters governing the vibration of wheel–rail systems are the wheel–rail combined roughness[1, 6], the track decay rate[1, 7] (TDR) and other track dynamic parameters such as the stiffness and damping of the rail pads. The wheel dynamics also play a role. To establish a noise prediction model it is necessary to quantify these critical parameters. In practice, they are often chosen from experience, existing standards or measurements conducted on other tracks. This inevitably leads to disagreement between the measured and predicted noise, which is often attributed to uncertainties of these parameters. In order to reduce the uncertainties, it is important to be able to estimate the track parameters and combined roughness case by case. Other reasons to estimate these parameters include monitoring the growth of roughness or irregularities and assessing the deterioration of track structures in the management and maintenance of railway lines.

The stiffness and damping of rail fasteners can be measured in the laboratory by using a direct method[8] or an indirect method[9-11]. Thompson and Verheij[10] compared the stiffness and damping of unloaded rail fasteners derived from laboratory tests and field measurements. They observed large discrepancies between these two methods for the estimation of loss

factors of the fasteners although they found better agreement with regard to the stiffness. This illustrates a difficulty in using laboratory tests to quantify the behaviour of fasteners installed in track. In addition, the fastener stiffness and damping generally depend strongly on load[11, 12] and to a lesser extent on temperature[13] and frequency[14, 15], which brings difficulty and uncertainty in the parameter estimation even for the same track.

The TDR is a derived parameter of the track that has a direct influence on the noise produced by the rail[7]. The estimation of it using the hammer impact method has been standardised in EN 15461: 2008[16]. This test is quite time–consuming because it must include dozens of hammer positions and several repeated measurements per position on an unoccupied track; it also requires a degree of expert knowledge to analyse the data. An alternative way to measure the TDR is the train pass–by method developed by Janssens et al.[6]. They observed that the TDRs obtained from the pass–by method were generally larger than those from the impact hammer method and they attributed this difference to the pre–load applied to the track under passing trains. Li et al.[17] compared the TDRs obtained from the impact hammer method and train pass–by method and also found the pass–by method gave larger TDRs at most frequencies. Dittrich et al.[18] recently named this method the energy iteration method and conducted extensive benchmark tests to validate it. Their results, however, showed that the impact hammer method and energy iteration method matched well with each other irrespective of different loading conditions of the track. As the two methods have their own advantages and disadvantages, and measurement noise will definitely influence the measurements in either case, it is hard to tell which one is superior to the other from a comparison of them at a certain track site.

The roughness on the surface of the rail and wheel has a random profile; it also varies over time due to wear and grinding operations[19, 20]. The rail roughness required for rolling noise predictions can be measured either by systems based on a short stationary beam

mounted above the rail or a portable trolley moving along the rail[21, 22]. Wheel roughness can be measured by a displacement transducer as long as the wheel is allowed to turn freely above the rail[1]. For the rail roughness, ISO 3095: 2013[23] specifies the longitudinal and lateral positions to be measured and the associated data processing method. However, differences in the operation of the equipment in the field and post–processing of the measured data will lead to variations in the measured roughness spectra for the same track[24]. It is clear therefore that the direct measurement of combined roughness requires great effort and specific facilities.

As the wheel–rail contact exists over a finite length and width, roughness with short wavelengths tends to be attenuated in the effective excitation of the wheel–rail system[1]. This is the so called contact filter effect. Remington[25] proposed an analytical filter function to represent it. The simplified form of the function can be written as[1]

$$\left|H\left(k\right)\right| = \left(1+\frac{\pi}{4}\left(ka\right)^3\right)^{-0.5} \tag{1}$$

where $k$ is the wavenumber of roughness in the longitudinal direction and $a$ is the half-length of the contact patch. Remington and Webb[26] later developed a numerical model to approximate the contact area by a series of distributed point–reacting springs. This model allows the contact filter effect to be evaluated in the time domain based on the measured roughness. Thompson[1, 27] made a comparison between the numerical and analytical models and found that the simple filter function could be used reliably up to about $ka$=6.5.

To avoid the direct measurement of roughness and evaluation of the contact filter effect, Dittrich and Janssens[28] initially proposed an idea for indirect measurements of the combined effective roughness from rail vibration with the help of the estimated TDR. Janssens et al.[6] then developed this method by using the measured rail vibration under train pass–bys and compared it with the direct method. They found the pass–by method gave a similar roughness spectrum shape to that from the direct measurement. Dittrich et al.[18] showed that the position

of the accelerometer on the rail had an insignificant effect on the estimated roughness for wavelengths greater than 10 mm.

Standardisation work[18] has been undertaken to implement the indirect train pass–by methods in a new standard for measuring the TDR and combined roughness. Although many field tests have been conducted to validate the pass–by methods, few numerical or theoretical studies have been carried out to investigate the applicability and limitations of these methods. This study therefore aims to illustrate the assumptions and limitations of the methods through analytical, numerical and experimental analyses, and to provide some principles in their use. In addition, new alternative procedures are also adopted and compared with the existing methods.

The estimation of track parameters and combined roughness from rail vibration measured in the field relies on the use of theoretical or numerical dynamic models for the track and the wheel. A rail is often represented by an infinite Timoshenko beam on a continuous support[1, 3] in the prediction of rolling noise. The advantage of this model lies in its analytical solution. To include the pinned–pinned effect near 1000 Hz, it is better to use an infinite Timoshenko beam on discrete supports[1]. One possible way to obtain the numerical solution for this track model is to use a finite number of elastic supports to approximate the infinite supports[29].

The cross–sectional deformation of the rail becomes significant at frequencies above 1500 Hz. Wu and Thompson[30] proposed a simple approach to represent the cross–sectional deformation by means of a composite beam. However, Jones et al.[7] showed that this model failed to give accurate TDRs at 5000 Hz compared with the measured ones. Nilsson et al.[31] established a wavenumber finite element (WFE) model of a rail on a continuous foundation to predict rail vibration and noise. Ryue et al.[32] used this model to simulate TDRs up to 80 kHz. The WFE model of the rail on a continuous support suits the simulation of high frequency vibration of the rail but neglects the pinned–pinned effect. Here, this model is extended to

include periodic supports.

The structure of the paper is organized as follows. First, a train–track interaction model is proposed for the simulation of rail vibration by using the WFE model of the rail extended to include discrete supports. This accounts for the pinned–pinned mode of the rail around 1000 Hz as well as cross–sectional deformation of the rail at higher frequencies. Second, simulated rail vibration with assumed measurement noise is used to illustrate the applicability of the direct and indirect methods for the estimation of TDR. This is followed by a case study based on field measurements on a ballasted track in the UK. Third, a procedure is presented to identify the stiffness and damping of the rail pad and ballast, and damping of the rail from hammer impact measurements. Then, the train pass–by method for the estimation of combined roughness is introduced and various simplifications are discussed with emphasis on their assumptions and accuracy. A comparison is afterwards made between the estimated roughness and the directly measured one. Finally, the main conclusions are drawn in the last section. Only vibration in the vertical direction is considered, although the same methods could also be applied to lateral vibration.

## Model for the simulation of rail vibration

### *Track model*

A WFE[31] model representing a free rail of infinite length is first developed to account for bending, shearing and cross–sectional deformation of the rail. To allow for the discrete supports of the rail provided by the fasteners, sleepers and ballast, a finite number of frequency–dependent support springs are then introduced. At the location of each rail fastener, the supports are distributed across the rail foot (Fig. 1(a)-(b)).

To obtain the vibration of the discretely supported rail under a given external vertical force, a compatibility equation is required either in terms of unknown rail displacements[1, 29] at

the support points or unknown reaction forces[33, 34] of the support springs. By using the latter method[33, 34], the compatibility equation of the discretely supported rail for harmonic motion at angular frequency $\omega$ is expressed as

$$\left[\mathbf{Y}_{\mathrm{rf}}(\omega)+\mathbf{Y}_{\mathrm{s}}(\omega)\right]\mathbf{F}(\omega)+\mathbf{Y}_{\mathrm{P}}(\omega)P=\mathbf{0} \tag{2}$$

where $\mathbf{F}(\omega)$ denotes a vector of unknown reaction forces at the rail support locations; $\mathbf{Y}_{\mathrm{s}}(\omega)$ is a diagonal matrix containing the mobility of each support spring, each of which in the case of a ballasted track can be expressed as a frequency–dependent function[1] of the stiffness and damping of the rail pad and ballast, and mass of the sleeper; $\mathbf{Y}_{\mathrm{P}}(\omega)$ represents a vector of mobilities of the free rail at the positions of the springs due to the external load *P*; and $\mathbf{Y}_{\mathrm{rf}}(\omega)$ represents the mobility matrix of the free rail due to forces at the positions of the springs.

In order to evaluate $\mathbf{Y}_{\mathrm{P}}(\omega)$ and $\mathbf{Y}_{\mathrm{rf}}(\omega)$, the stiffness, mass and damping matrices of the WFE model of the free rail are firstly assembled in the WANDS program[35]. Then the residual method[31] is applied to calculate the mobilities of the free rail subjected to a point force at the rail head node and each node of the rail model corresponding to a support spring. After obtaining the solutions for the unknown reaction forces **F** from Eq. (2) for a unit external force *P*, the point and transfer mobilities of the discretely supported beam can be calculated for various response points[33, 34].

*Wheel–rail interaction model*

To simulate the rail vibration due to a passing train, wheel–rail contact forces under the excitation of combined roughness should be obtained. It is generally necessary to take into account the effect of multiple wheels on the rail at least in the frequency ranges where the TDR is low. This can be realized by considering one wheel as the active wheel with roughness excitation and treating the others as passive wheels coupled to the track without

roughness excitation[36]. Treating the *i*th wheel as the active one, a roughness of complex amplitude $R_i$ is introduced at this wheel–rail interface. The wheel–rail interaction is then realized through a matrix formulation of the compatibility of the wheel–rail displacement as

$$\left[\mathbf{Y}_{\mathrm{rh}}+\mathbf{Y}_{\mathrm{c}}+\mathbf{Y}_{\mathrm{w}}\right]\mathbf{F}_{\mathrm{c}}^{i}=j\omega\begin{Bmatrix}0\\ \vdots\\ 0\\ R_i\\ \vdots\\ 0\end{Bmatrix} \tag{3}$$

where $\mathbf{F}_{\mathrm{c}}^{i}$ represents the wheel–rail contact forces at all the wheels in the vertical direction induced by the combined roughness at the *i*th wheel–rail interface; the element $Y_{\mathrm{rh},ik}$ in $\mathbf{Y}_{\mathrm{rh}}$ stands for the transfer mobility corresponding to the rail head at the locations of the *k*th and *i*th wheels, which varies depending on the position of the wheel on the discretely supported rail; $\mathbf{Y}_{\mathrm{c}}$ is a diagonal matrix denoting the mobility of the linearized Hertzian contact spring; $\mathbf{Y}_{\mathrm{w}}$ is a diagonal matrix of the wheel mobility which can be calculated using a rigid wheel model or from a finite element model of a flexible wheel[1].

In the following simulation of rail vibration it is assumed that each $R_i$ is incoherent[36] and has the same spectrum. Moreover, $R_i$ represents the effective roughness that is obtained from the actual roughness profile with application of the contact filter effect expressed by Eq. (1).

The total amplitude of the wheel–rail contact force $F_{\mathrm{c}n}$ at the *n*th wheel, caused by roughness at all the wheels, can be expressed as the energy summation of the incoherent excitations

$$F_{\mathrm{c}n}=\sqrt{\sum_{i=1}^{N}\left|F_{\mathrm{c}n}^{i}\right|^{2}} \tag{4}$$

where $N$ is the number of wheels in the train on the rail; and $F_{cn}^{i}$ is an element in vector $\mathbf{F}_{\mathrm{c}}^{i}$ denoting the wheel–rail contact force at the $n$th wheel due to roughness excitation at the $i$th wheel. The wheel–rail contact forces under each wheel in the given frequency band are generally different for each position of the wheels.

If the interference between the wheels on the same rail is neglected, the non–diagonal elements in $\mathbf{Y}_{\mathrm{rh}}$ become zeros and the summation in Eq. (4) is not required. Moreover, if in addition the driving point mobilities of the rail are assumed not to vary with position, as would be the case for a continuously supported rail, then the contact force $F_{cn}$ at each wheel has the same magnitude at a given frequency.

*Rail vibration during a train pass–by*

Since the train speeds are generally far smaller than the wave propagation speeds along the rail, the Doppler effect can be ignored in the calculation of the rail vibration. The wheels are assumed to be stationary but the effect of wheel motion is simulated by averaging the response for a set of different wheel positions. The instantaneous rail velocity amplitude at a sensor position can be therefore expressed by

$$V_{\mathrm{s}} = \sqrt{\sum_{n=1}^{N} F_{cn}^{2} \left| Y_{\mathrm{rs}n} \right|^{2}} \tag{5}$$

where $Y_{\mathrm{rs}n}$ denotes the transfer mobility of the rail at the sensor position produced by a unit force on the rail head beneath the $n$th wheel. $V_s$ is a function of the longitudinal distance between the fixed sensor and the wheel at different positions.

In the rest of the paper this model, with and without the simplifying assumptions listed above, is used to assess different methods of determining TDR and combined roughness.

## Estimation of TDR

*Field test and parameters used in the simulation*

In this section, the direct impact hammer method and two indirect train pass–by methods for determining TDRs will be discussed with the help of the model proposed in the previous section. A hammer impact measurement for TDR was conducted in May 2015 for a ballasted track with UIC60 rails and bi–block sleepers. The rail vibration of the same track section was recorded in December 2015 under four train passages each comprised of 6 cars at operational speeds from 212 km/h to 218 km/h. These field measurement data will be discussed in the case study parts of this section and the Section 'Estimation of combined roughness'.

Table 1 lists four sets of arbitrarily chosen parameters for ballasted tracks that will be used in the simulation of rail vibration; the fifth column will be discussed later. The four tracks with significantly different rail pad stiffness are referred to as stiff, medium, soft and very soft for convenience. The sleeper mass per rail was set to 120 kg. The WFE model of a UIC60 rail attached to discrete supports was used for all tracks (Fig. 1). Each rail support was discretized by 8 springs across the rail foot. In this study the stiffness of each spring was simply determined in accordance with the transverse length of rail to which it is attached. This method of distributing the spring stiffness has been compared with a more sophisticated method considering the shape function of the quadrilateral element and found to give almost identical results for the mobility at the rail head. The supports of the infinite rail were truncated in the longitudinal direction into a total of 131 rail supports with a fastener spacing of 0.6 m. This allows the typical waves generated in the centre of the supported section of the rail to attenuate to sufficiently small amplitude at the ends of the finite supported region. To consider different positions of the impact hammer or the wheels along the rail, the transfer mobilities of the rail were obtained every 0.1 m over the discretely supported section of the rail, subjected to a driving force located at 0.1 m intervals within one fastener span (Fig. 1).

A total of 24 wheels distributed over 120 m along the rail were considered in the

wheel–rail interaction analysis to comply with the configuration of the measured train. Fig. 2 shows the magnitude of the sum of the mobilities of the wheel and the contact spring. Both rigid and flexible wheel models are considered. It can be seen from Fig. 2 that the flexible wheel model exhibits many resonance peaks and anti–resonance dips in the mobilities above 2000 Hz. The rigid wheel model is a good approximation to represent the averaged mobilities of the flexible wheel model over a wide frequency range. Since the estimation of TDR is dependent on the relative magnitude of the rail vibration along the track during the passage of the train, the details of the wheel mobility are not important and the rigid wheel model was used in this section for the simulation of rail vibration. Calculations were carried out at one–ninth octave frequency spacing (i.e. 30 points per decade). The flexible wheel model will be applied in the Section 'Estimation of combined roughness' associated with the narrow frequency spacing to obtain more accurate rail vibration considering the resonances of the flexible wheel. In each case the simulated results are ultimately converted to one–third octave band resolution for further processing.

*Impact hammer method*

In the impact hammer measurement, according to EN 15461: 2008[16] the TDR $D$ expressed in dB/m in each one–third octave band is evaluated using the following formula

$$D = \frac{4.343}{\sum_{i=0}^{M} \left| \frac{Y_i}{Y_0} \right|^2 \Delta x_i} \tag{6}$$

where $Y_i$ is the measured frequency–response function (or transfer mobility) in each one–third octave band due to the impact force at the $i$th hammer position; the subscript $i$=0 denotes the sensor position; $M$+1 is the total number of hammer positions; and $\Delta x_i$ is the weighted interval in metres for each hammer position.

Fig. 3 illustrates the simulated vertical rail mobilities of the stiff track using the model

shown in Fig. 1. Fig. 3(a) shows the mobilities at $x$=0 and Fig. 3(b) shows the corresponding results for excitation at 0.3 m (the position of the first sleeper). Fig. 3(c) and Fig. 3(d) show the results at 1.25 kHz and 5 kHz respectively as a function of hammer position. It can be seen that the mobilities at the rail head above 1000 Hz are obviously different from those at the rail foot due to the cross–sectional deformation of the rail. Note that the sensor location on the rail foot has been chosen to be slightly away from the centreline. These differences lead to different estimated TDRs, as shown in Fig. 4, if the vibration sensors are placed on the rail head or foot, especially at high frequencies.

Besides the effect of sensor positions, another potential challenge is the influence of background noise or instrumentation noise in the low frequency range. Fig. 5 compares the simulated rail foot mobilities of the stiff track with a real example of measurement noise which was obtained from the ambient vibration signal of the rail obtained during a hammer impact test. It can be noticed that the rail mobilities at low frequencies would be significantly affected by such inherent measurement noise. It is not surprising that the dips of the rail mobilities and the far–field transfer mobilities where the TDR is high are more vulnerable to measurement noise. Fig. 6 shows that the TDR estimated using the polluted rail mobilities deviates significantly from the correct one below 100 Hz.

To reduce this effect, it is possible to use two impact hammers, a large one with a soft tip to produce sufficient response at low frequencies and a smaller one with a hard tip for high frequencies. It is also important to avoid the use of the far–field rail mobilities at low frequencies in the estimation of TDR as these are easily contaminated. This can be achieved by setting a threshold (e.g. –15 dB) relative to the drive point mobility, below which the data are ignored. Additionally measured vibration data that are either too high or too low compared with the expected attenuation can be suppressed.

*Train pass–by method using energy iteration*

To illustrate the assumptions and limitations in the train pass–by method[18] for the estimation of TDR, a derivation of this method is given in this section. It is assumed first that the wheel–rail contact forces at all wheels are of same magnitude (see the assumptions after Eq. (4)), i.e. neglecting the interference between wheels and variations in the rail mobility with distance. Second it is assumed that, in a given frequency band, the dependence of the rail vibration induced by each wheel on the distance along the rail can be described by a decaying exponential function. Then the rail vibration 'energy' $E_{L_1}^{in}$ measured at a fixed position produced by the *i*th wheel, during the passage of the *n*th wheel over a distance $L_1$ (see Fig. 7) centred at the sensor position, can be written as

$$E_{L_1}^{in} = \int_{-L_1/2}^{L_1/2} \left( V e^{-\beta|x-x_{in}|} \right)^2 dx \tag{7}$$

where $V$ is the root mean square (rms) amplitude of rail vibration just beneath a given wheel; $\beta$ is related to the TDR by $D = (20\lg e)\beta = 8.686\beta$; and $x_{in}$ is the distance between the *n*th and *i*th wheels. If $L_1$ is less than the minimum distance between two wheels, Eq. (7) can be expressed as

$$E_{L_1}^{in} = \begin{cases} \dfrac{e^{\beta L_1} - e^{-\beta L_1}}{2\beta} V^2 \, \mathrm{e}^{-2\beta|x_{in}|}, & i \neq n \\ \dfrac{1 - e^{-\beta L_1}}{\beta} V^2, & i = n \end{cases} \tag{8}$$

The rail vibration energy $E_{L_1}^{n}$ induced by all the wheels during this time in which the *n*th wheel passes over the sensor position can be obtained by the summation of the vibration energy as

$$E_{L_1}^{n} = \sum_{i=1}^{N} E_{L_1}^{in} \tag{9}$$

Summing this total rail vibration energy over all $N$ sections of length $L_1$ corresponding to

the passage of each wheel over the sensor gives

$$E_{L_1} = \sum_{n=1}^{N} E_{L_1}^{n} = \frac{1-e^{-\beta L_1}}{\beta} V^2 \psi \tag{10}$$

where

$$\psi = \sum_{n=1}^{N} \sum_{i=1}^{N} \xi_{in} e^{-2\beta|x_{in}|} \tag{11}$$

$$\xi_{in} = \begin{cases} \dfrac{e^{\beta L_1} - e^{-\beta L_1}}{2\left(1-e^{-\beta L_1}\right)}, & i \neq n \\ 1, & i = n \end{cases} \tag{12}$$

If $\beta L_1 \gg 1$, $\xi_{in}$ also approaches unity in the case of $i \neq n$, as presumed by Dittrich et al.[18]

When the integral distance used to determine the vibration energy becomes sufficiently large (for example, if it is taken to be equal to the total length of the train $L_2$), the total vibration energy caused by all *N* wheels can be approximately expressed as

$$E_{L_2} \approx N \int_{-\infty}^{+\infty} \left(Ve^{-\beta|x|}\right)^2 dx = N \frac{1}{\beta} V^2 \tag{13}$$

Thus the parameter $\beta$ can be obtained by dividing Eq. (10) with Eq. (13)

$$\beta = \frac{-\ln\left(1 - \dfrac{E_{L_1} N}{E_{L_2} \psi}\right)}{L_1} \tag{14}$$

It is noted that $E_{L_1}$ and $E_{L_2}$ can be calculated in each frequency band from the measured rail vibration. As $\psi$ is itself a function of $\beta$, Eq. (14) has to be solved by an iteration algorithm. It is therefore called the energy iteration method by Dittrich et al.[18].

The estimation of the TDR from Eq. (14) is independent of the absolute rail vibration amplitude *V*. This allows the estimation of the TDR without a detailed knowledge of the track, the train or the roughness. Another advantage of this method lies in the fact that it takes into account the rail vibration contributed separately by each wheel using the factor $\psi$ in Eq.

(11). However, there are also several limitations in the method. In practice, $E_{L_1}$ is mainly determined by the attenuation of the rail vibration close to the excitation points while $E_{L_2}$ is determined by the averaged attenuation rate over a long distance. The value of $\beta$ may differ in these two regions so that Eq. (7) is not valid and the elimination of $\beta$ by dividing Eq. (10) by Eq. (13) is not rigorous. As a result, the main estimation error from the energy iteration method occurs due to neglecting the rapidly decaying evanescent waves that exist near the excitation points and the variation of the attenuation rates along the track in a given frequency band (see Fig. 3(c) and Fig. 3(d)). Other estimation errors are introduced by the differences between the vibration caused by each wheel due to the coupling effect of multiple wheels and the fact that the combined roughness under each wheel is non–stationary. In addition, the time–history of measured rail vibration during the passage of a wheel is strongly dependent on the actual roughness waveform in the vicinity of the sensor (see Fig. 7). This effect is ignored in the frequency domain based analysis. Nevertheless, the use of the averaged result from several train pass–bys can reduce this adverse effect to some extent.

Fig. 8 depicts the simulated instantaneous rail foot acceleration levels in three frequency bands during the passage of a train (a) without and (b) with assumed measurement noise. It can be noticed that the vibration of the rail decays at different rates as the train passes. The acceleration levels at 1250 Hz also fluctuate periodically due to the pinned–pinned effect (see Fig. 3(c)). Moreover, there are sharp peaks in the acceleration levels at each wheel position at 5000 Hz which indicate that the rail mobility is dominated by different waves in the near– and far–fields (see also Fig. 3(d)). This phenomenon is not consistent with the assumption of an exponential decay in the energy iteration method.

Fig. 9 shows the simulated TDRs obtained using the hammer impact method and the energy iteration method for the four different sets of track parameters in Table 1. From this, it

is clear that there are considerable discrepancies between the estimated and directly calculated TDRs from Eq. (6) even without any measurement noise. A Gaussian noise with standard deviation 10% of the maximum simulated acceleration amplitude in each frequency band is further introduced to all the simulated accelerations together with a wheel position identification error with a standard deviation of 0.1 m in the calculation of $E_{L_1}$ (i.e. the interval of the integral is not centred at the exact wheel position). The estimated TDR with measurement noise shown in Fig. 9 is the averaged result from five simulations with different random noise samples. It can be seen from the figure that the energy iteration method is quite robust at frequencies between 500 Hz and 3000 Hz for the four different tracks but is inaccurate for the higher values of TDR at low and high frequencies. Fig. 10 shows the effect of reducing the integral distance $L_1$ by half while keeping the same amount of measurement noise. This shows that the estimation quality can be improved between around 300 Hz and 500 Hz for the case with measurement noise.

*Train pass–by method using slope fitting*

According to its definition, another way to estimate the TDR is to obtain the slope of the rail vibration level curve over a certain distance $L_3$ (see Fig. 8(c)) after a passage of a wheel. To apply this method, the rail acceleration levels should be obtained at short time intervals corresponding to the motion of the train by steps of e.g. 0.1 m. The time instant must also be detected when the relevant wheel is just passing over the sensor position on the rail. Then the linear fitting can be conducted on the time–history of the rail acceleration levels over a larger distance $L_3$ starting from the detected time instant. The TDR is just the absolute value of the fitted slope.

Fig. 11 shows the estimated TDRs obtained from slope fitting of the simulated rail foot acceleration levels including the same measurement noise as those considered in the simulations of the energy iteration method. It can be observed that the slope fitting method

with $L_3$ =1.2 m gives a similar estimate to the energy iteration method with $L_1$ =1.0 m. A good estimation in the regions with high decay rates at low and high frequencies can be obtained by reducing $L_3$ to 0.6 m. However, a small value of $L_3$ leads to overestimation of the low TDRs in the middle frequencies around 1000 Hz. It is suggested to use a smaller value of $L_3$ for frequencies with high decay rates and a larger one for frequencies with low ones to obtain the decay rates more reliably in all frequency bands.

*Case study*

Fig. 12(a) shows a time–history of vertical acceleration measured on the rail foot during the passage of a train with a speed of 218 km/h. Fig. 12(b) and (c) illustrate the rail acceleration after low–pass filtering with a cut–off of 100 Hz. The filtered acceleration curve keeps the low frequency rail vibration content with high decay rates, and it can be used to identify the time instants when the wheels passed over the measurement position. Fig. 12(d) shows the measured rail acceleration levels during the motion of the train, with an averaging time corresponding to a distance equal to one sleeper span (0.6 m). The comparison between the measured vibration levels and the simulated ones shown in Fig. 8 suggests that the measured results are highly polluted by background or instrumentation noise. This might bring significant error in the estimation of TDRs using the pass–by methods. Other factors affecting the accuracy of estimation include the inhomogeneity of the track properties and non-stationary random roughness occurring in reality.

Fig. 13 gives the estimated TDRs measured at this site from the hammer impact method and pass–by methods. It can be seen from Fig. 13(a) that the directly measured TDR is incorrect below 400 Hz if it is obtained from Eq. (6) by using the results for all the hammer positions. The trends are similar to the simulated results in Fig. 6 when measurement noise is included. Results are also shown in which the highly polluted far–field transfer mobilities are excluded from the summation in Eq. (6) by setting thresholds. These have been chosen to

exclude the transfer mobilities below 400 Hz corresponding to attenuation rates relative to the driving point mobility greater than 30 dB/m or less than 3 dB/m. This leads calculated TDR much closer to those expected from experience. The above threshold values were selected because the TDRs below the cut-on frequencies of the ballast track are generally no more than 20 dB/m or less than 6 dB/m, according to the simulated TDRs for different tracks in this study as well as those for ballast tracks provided in existing literature[1]. Other threshold values or criteria for excluding mobilities can be used if the track property is largely known or the measurement noise can be quantified. In any case, the TDRs at low frequencies are still unreliable if the measurement noise plays a significant role, because only the transfer mobilities corresponding to a few hammer positions can be used in the calculation with the threshold method.

Fig. 13(b) shows results from the energy iteration method using different integration lengths $L_1$. The results at high frequencies are quite stable even when $L_1$ is varied. Since a large value $L_1$=2.0 m fails to predict the peak at 1250 Hz and a small value $L_1$=0.6 m may be too short to represent the vibration energy, an integral distance $L_1 = 1\,\text{m}$ was adopted for the final estimated decay rates in this study. Fig. 13(c) shows the results of the slope fitting method. This also gives stable results at high frequencies with different fitting distances. The fitting distance $L_3$=1.2 m is therefore used for the frequencies above 1000 Hz and $L_3$=0.6 m for those below 1000 Hz where the TDR is higher.

The TDRs estimated from the above three methods are compared in Fig. 13(d). It can be seen that the estimated TDRs from the two pass–by methods agree with each other to some extent but they do not match well with the result obtained from the hammer impact method. This may be attributed to the following reasons: (1) the impact hammer method gives the TDR for an unloaded track but the pass–by methods give the results for a loaded track; (2) the

track parameters may have changed between May and December 2015, particularly due to the change in temperature[13]; (3) some measurement noise and background noise will lead to estimation errors; and (4) all three methods have their own limitations and assumptions shown in the previous numerical and analytical discussions.

**Estimation of track stiffness and damping**

Besides the TDR, the values of the stiffness and damping parameters of the track are generally required for use in numerical models for rolling noise prediction. The impact hammer measurements not only give the decay rates of the track but can also be used to determine important information such as the rail pad stiffness and damping loss factor. This section will present a general procedure to estimate these track parameters from the impact hammer measurements.

Firstly, the peak frequencies in the driving point mobility can be used to obtain the rail pad stiffness and ballast stiffness by comparison with a model. Fig. 14(a) shows the measured driving point mobility of the rail head together with the simulated ones for various track parameters. The peak in the measured mobility at 630 Hz indicates the rail pad stiffness should be around 600 MN/m as represented by the stiff track in Table 1. This peak frequency indicates the resonance frequency of the rail mass on the support stiffness of the rail pad[1]. The peak of the measured mobility around 90 Hz shows that the ballast stiffness per fastener should be around 48 MN/m. This peak frequency represents the resonance frequency of the mass of the rail plus the sleeper on the elasticity of the ballast.

Secondly, the magnitude and sharpness of the peaks in the driving point mobility can be utilized to estimate the damping loss factors of the rail pad and ballast. Fig. 14(a) illustrates that in this case the loss factor of the rail pad of the track must not be as small as 0.05 if the magnitude and sharpness of the simulated peak mobility is to match the measured ones. By

trial and error, the required loss factor of the rail pad can be determined as 0.25 and that of the ballast as 1.0 in this example.

Third, the TDR can be used to derive a value for the equivalent loss factor of the rail. It can be observed from Fig. 14(a) that the rail loss factor does not have a significant effect on the point mobility, whereas it has a significant effect on the TDR at high frequencies. As shown in Fig. 14(b), the loss factor of the rail can be estimated as 0.01 to match the simulated and measured decay rates in the high frequency range around 3000 Hz. As reported by Ryue et al.[32], the damping loss factor of the rail itself can be as low as 0.0002, since the material damping of steel is quite low. The estimated rail loss factor of 0.01 here is mainly due to the dissipation of vibration energy by the connection of the rail foot with the fasteners which are not included in the model.

Finally, the simulated TDR and mobilities should be checked against the measured results over a wide frequency range and if necessary the estimated parameters adjusted slightly to obtain a better agreement with the measured curves. The agreement between the simulated and measured TDRs in Fig. 14 shows that the estimated track parameters are reasonable. The agreement at the peak at 1250 Hz corresponding to the pinned–pinned effect also gives confidence in the estimated parameters. Nevertheless, it is not considered necessary to match the simulated peak in the TDR to the measured one around 400 Hz, because the measured decay rate at this frequency is more likely to be affected by measurement noise as shown in Fig. 6 and Fig. 13(a). Although the measured TDR below 400 Hz has been improved by excluding highly polluted far–field transfer mobilities, it is still unreliable because only transfer mobilities corresponding to a few hammer positions could be used in the calculation. No obvious improvement was found by applying wavelet filtering to the measured data, because the measurement noise is either quite small compared with the driving point mobility or very large compared with the far–field transfer mobilities. The fifth column

of Table 1 gives the estimated parameters for the test track obtained from the fitting procedure. Note that these values are obtained without the train loading. These values will be applied in the next section for the estimation of wheel–rail combined roughness. As the estimated TDRs from the pass–by methods show no obvious peaks and dips (see Fig. 13(d)), they are not suitable for the parameter extraction of the loaded track.

Fig. 15 shows the calculated mobilities and TDRs for the estimated track parameters from the WFE rail attached to discrete supports, and the infinite Timoshenko beams on discrete and continuous supports together with those from measurements. It can be noticed from Fig. 15(a) that the peak frequency of 630 Hz (cut–on frequency of the track) in the mobility curve obtained from the WFE model shifts to 680 Hz and 736 Hz in one–ninth octave resolution if the two Timoshenko beam models are used instead. This will lead to an underestimation of 16% and 36% for the rail pad stiffness if the discretely and continuously supported Timoshenko beam models are respectively applied in the curve fitting. Nevertheless, if these models are to be used, the corresponding parameters would be the correct ones to use with them. In fact it is found that the calculated cut–on frequencies from the three models will show less difference if the pad stiffness is softer. Moreover, it can observed from Fig. 15(b) that the Timoshenko beam models underestimate the TDRs in the frequency range from 3 kHz to 7 kHz. A larger loss factor of the rail can be assigned to the Timoshenko beam in order to match the simulated TDR with the measured one in this frequency range, but it does not represent any physical damping in the track. On the other hand, the use of a more advanced track model, i.e., the WFE model of a free rail attached to discrete supports, can give better simulated TDR with peaks and dips that agree with the measured ones. In conclusion, it is very important to use an appropriate track model in the estimation of track parameters from curve fitting. The use of the WFE model of the rail is recommended when the frequency of interest is above 3 kHz or when the cut–on frequency of the track approaches the

pinned–pinned frequency in the case of stiff fasteners. In the latter case, a discrete support is also suggested in the track model as presented in this study.

## Estimation of combined roughness

The magnitudes of the wheel–rail contact force and of the rail vibration in the vertical direction are both linearly dependent on the magnitude of the wheel–rail combined roughness, as indicated by Eqs (2)–(5). This relationship provides the possibility to estimate the roughness from measured rail vibration during a train pass–by. In this section, a full method using the proposed numerical model for rail vibration is applied to estimate the combined roughness. The results are compared with those obtained from the simplified method introduced by Janssens et al.[6] and Dittrich et al.[18] and described in this section. The estimation errors arising from the two methods are discussed through numerical simulations. In June 2015, the rail roughness was measured using a portable CAT trolley[22] on the same section of the track as the rail vibration measurements. Wheel roughness has also been measured for 64 wheels from trains of the type running over the section, although they were not necessarily the ones used in the pass–by measurement. The directly measured rail and wheel roughness levels and their sum are depicted in Fig 16. It can be observed that the rail roughness dominates at wavelengths between 20 mm and 40 mm and above 300 mm but the wheel roughness has an important contribution to the combined roughness at wavelengths between 50 mm and 300 mm. The directly measured combined roughness is compared with the estimated results obtained from the pass–by methods.

*Full method*

If the track parameters are determined or at least estimated with reliable accuracy, the combined wheel–rail roughness $r$ can be estimated from the measured rail vibration levels as

$$20\log_{10}\frac{r}{r_0} = 20\log_{10}\frac{v_m}{v_0} - 20\log_{10}\frac{v_s}{v_0} + 20\log_{10}\frac{r_s}{r_0} \tag{15}$$

where $v_m$ is the measured rms value of rail velocity in each one–third octave frequency band; $v_s$ is the simulated rms velocity obtained using the given roughness $r_s$ and track parameters; $r_0$ and $v_0$ are reference values for the calculation of roughness level and vibration level respectively. It is noted that $r$ and $r_s$ are both expressed here as functions of frequency but can be readily expressed in terms of wavelength for a given train speed.

The accuracy of the estimated roughness is obviously dependent on the accuracy of the measured rail vibration. However, the main error of the estimation comes from the simulated rail vibration which relies on the numerical model and the input parameters, especially the TDR. To quantify the estimation error due to inaccuracy in track parameters, the rail foot vibration was first simulated with the aforementioned model, the direct roughness and the 'estimated' track parameters listed in Table 1 for a train speed of 215 km/h. This is treated as the measured rail vibration in Eq. (15). Then, the rail vibration was simulated with inaccurate track parameters by varying them around the given ones with certain factors of 0.63, 0.80, 1.26 and 1.60. The estimation error could be obtained from Eq. (15) by subtracting the vibration level (representing the measurement) under given track parameters with that (simulated) using inaccurate parameters. Fig. 17 shows the influence on the estimated roughness of changes in the various track parameters, i.e. pad stiffness and loss factor and ballast stiffness and loss factor. It can be seen from Fig. 17 that the pad stiffness has the most significant effect on the estimated roughness over a wide range of wavelengths. The loss factor of the rail pad mainly affects the estimated roughness for wavelengths less than 100 mm whereas the ballast stiffness and damping significantly influence the results for wavelengths larger than 200 mm. Generally, the maximum estimation error in the roughness reaches ±2 dB when the error in each track parameter is ±25%.

*Simplified method*

By assuming the forces due to all wheels are incoherent and the rail mobilities do not vary with the wheel positions, the simplified method of Janssens et al.[6, 18] is obtained. The rms rail vibration averaged over the pass–by time of a train can be obtained from Eqs. (1) – (5) and Eq. (13) as

$$v_{\mathrm{s}} = \sqrt{\left|\frac{j\omega r_{\mathrm{s}} Y_{\mathrm{s}}}{Y_{\mathrm{rh}} + Y_{\mathrm{w}} + Y_{\mathrm{c}}}\right|^2 \frac{N}{\beta L_2}} \tag{16}$$

where $Y_{\mathrm{rh}}$ denotes the rail head mobility at the driving point; $Y_{\mathrm{s}}$ is the transfer mobility to the rail foot sensor position for excitation at the same longitudinal position; and $Y_{\mathrm{w}}$ and $Y_{\mathrm{c}}$ are respectively the mobilities of the wheel and the wheel–rail contact spring. Substituting Eq. (16) into Eq . (15) gives

$$20\log_{10}\frac{r}{r_0} = 20\log_{10}\frac{v_{\mathrm{m}}}{v_0} + 10\log_{10}\frac{\beta L_2}{N} - A_1 - A_2 - A_3 - 20\log_{10}\omega - 20\log_{10}\frac{r_0}{v_0} \tag{17}$$

where $A_1 = 20\log_{10}\left|\frac{Y_{\mathrm{s}}}{Y_{\mathrm{rh}}}\right|$ represents the level difference between the vibration at the sensor position and the rail head at the driving point; $A_2 = 20\log_{10}\left|\frac{Y_{\mathrm{rh}}}{Y_{\mathrm{rh}} + Y_{\mathrm{w}} + Y_{\mathrm{c}}}\right|$ indicates the level difference between the combined roughness and the displacement at the rail head; and $A_3 = 20\log_{10}|H|$ accounts for the contact filter effect described by Eq. (1) and converts the combined effective roughness to combined roughness that is comparable to the directly measured one. In Janssens et al.[6, 18] $A_1$ was generally set to be 0 dB up to 4 kHz and $A_2$ was pre–calculated for particular situations with a continuously supported track model and a flexible wheel model. If the track parameters for a particular location are known, $A_1$ can be calculated from the WFE model of the rail on an equivalent continuous support, and $A_2$ can be also obtained from the same WFE model of the rail together with the flexible wheel model.

However, in order to illustrate the accuracy of the original method in references[6, 18], a continuously supported Timoshenko beam model of the rail was used in this study to obtain $A_2$. Fig. 18 shows the variation of $A_1$, $A_2$ and $A_3$ with frequency; the corresponding wavelength at a train speed of 215 km/h is also shown. They all have large effect on the estimated roughness at high frequencies around 6 kHz (or short wavelengths about 10 mm). Therefore, the accuracy of the simplified method is highly dependent on the models applied to obtain these values when estimating the roughness of short wavelengths. Eq. (17) becomes identical to that reported by Dittrich et al.[18] when $r_0$ and $v_0$ take the same values and the measured rail vibration is expressed in terms of acceleration level rather than velocity.

The advantage of this simplified method is that the measured track decay rate can be explicitly introduced into the roughness estimation. Nevertheless, other errors are introduced by the assumptions of incoherent wheels and invariant rail mobility and also from inaccuracies in the parameters $A_1$, $A_2$ and $A_3$ used in the calculation. Fig. 19 shows the error introduced by the simplified method when all the track parameters are known exactly. The TDR calculated from the WFE model of the free rail attached to discrete supports was utilized in Eq. (17) to represent the measured one. It can be seen from Fig. 19 that the simplified method overestimates the roughness by about 10 dB for a wavelength of 47 mm. This corresponds to 1250 Hz at the train speed of 215 km/h where the peak TDR due to the pinned–pinned mode occurs. The difference occurs because the simplified method neglects the pinned–pinned effect whereas the full method overestimates it by ignoring the longitudinal length of the rail pad. Other reasons leading to the estimation error of the simplified method are due to the assumptions of incoherent wheels and invariant rail mobility along the track. Fig. 19 shows that including $A_1$ has an obvious effect on the estimation above 4000 Hz, or for wavelengths smaller than 15 mm, which agrees with previous findings[6, 18]. At lower frequencies around 400 Hz, $A_1$ also has an influence of about 1.5 dB.

*Case study*

Fig. 20(a) compares the directly measured combined roughness with that estimated from the full pass–by method, using the estimated track parameters shown in the last column of Table 1. Note that there are significant variations between trains. The full pass–by method underestimates the roughness at most wavelengths. This may be attributed to the fact that the track stiffness and damping adopted in the simulation are obtained from the unloaded track. Fig. 20(b) shows the effects of increasing the pad and ballast stiffness by a factor of 3 in the simulation to approximate the effect of loading. As a result of this change the discrepancy between the measured roughness and estimated one is reduced.

Fig. 21 gives the estimated roughness obtained from the simplified method by using directly measured TDR or indirectly estimated TDRs in Eq. (17). It can be seen from the figure that the use of TDRs obtained from pass–by methods gives an estimated roughness that matches well with the directly measured one for wavelengths between 20 mm and 100 mm. However, the use of the TDR from the hammer impact method underestimates the roughness because the directly measured TDR on the unoccupied track is generally lower than the pass-by estimations for the loaded track (see Fig. 13(d)).

## Conclusions

Methods for the estimation of track parameters and wheel–rail combined roughness have been investigated in this study by using simulations based on a wavenumber finite element model of a free rail attached to discrete supports. This model allows for the effect of the pinned–pinned mode of the track and cross–sectional deformation of the rail above 1000 Hz. It has been utilized to simulate the rail vibration in the frequency domain due to a hammer impact or a train pass–by.

In the impact hammer measurements, the position of the vibration sensor was found to

have a significant effect on the measured track decay rates above 1000 Hz, particularly above 5000 Hz. The measured track decay rates in the low frequency range could be easily affected by unavoidable measurement noise. A method has been suggested to exclude far–field transfer mobilities of the rail to obtain the track decay rates at low frequencies.

In the estimation of track decay rates using the vibration during a train pass–by, it is found that the energy iteration method is likely to be accurate for low track decay rates but inaccurate for high track decay rates, whereas the slope fitting method was found to be more reliable than the energy iteration method in the frequency ranges with higher decay rates. The distances used for the energy integral and slope fitting in the two pass–by methods should be carefully chosen to improve the quality of the estimation.

A comparison has been made between the track decay rates estimated from the direct hammer impact method and indirect pass–by methods in a case study using field measurements. The differences between the results of direct and indirect methods may be associated with different loading and temperature conditions of the track.

A general procedure has been adopted to identify the stiffness and damping parameters of the unloaded track from the hammer impact measurement using a suitable track model. The stiffness of the rail pads and ballast was derived from the peak frequencies of the driving point mobility of the rail, and their damping was estimated by matching the magnitude and sharpness of the simulated rail mobility peak with the measured one. The directly measured track decay rates at high frequencies could be fitted using an equivalent loss factor of the rail of 0.01. However, the track parameters of the loaded track during the passage of a train could not be obtained from the indirectly estimated track decay rates because they showed no clear peaks or dips. This problem needs to be resolved with an improved estimation method and more accurate field tests in the future.

A full train pass–by method has been developed as an extension of the established

pass-by method to estimate wheel–rail combined roughness. It was found that the existing simplified method overestimates the roughness corresponding to the pinned–pinned resonance frequency of the rail. Nevertheless, the simplified method could give a good estimation of the roughness if the track decay rates estimated from train pass–bys are utilized. For further validation and improvement of the simplified method, a more advanced model of the track is required in the future that can allow for the unloaded and loaded regions under a running train. More field measurements should be also conducted to obtain the wheel roughness, rail roughness, and rail vibration at the same time to exclude the effect of changing track properties and roughness over time and temperature.

All data published in this paper are openly available from the University of Southampton repository at http://dx.doi.org/10.5258/SOTON/D0068.

## Funding

The study was supported by the China Scholarship Council, the Natural Science Foundation of Shanghai (No.15ZR1442800) and EPSRC under the grant EP/H044949/1, 'Railway Track for the 21st Century'.

## References

1. Thompson D. *Railway noise and vibration: mechanisms, modelling and means of control*: Elsevier, 2009.
2. Remington PJ. Wheel/rail rolling noise, I: Theoretical analysis. *The journal of the Acoustical Society of America*. 1987; 81: 1805-23.
3. Thompson DJ, Hemsworth B, Vincent N. Experimental validation of the TWINS prediction program for rolling noise, part 1: description of the model and method. *Journal of sound and vibration*. 1996; 193: 123-35.
4. Thompson D, Jones C. A review of the modelling of wheel/rail noise generation. *Journal of sound and vibration*. 2000; 231: 519-36.
5. Zhang XY, Squicciarini G, Thompson DJ. Sound radiation of a railway rail in close proximity to the ground. *Journal of Sound and Vibration*. 2016; 362: 111-24.
6. Janssens MHA, Dittrich MG, De Beer FG, Jones CJC. Railway noise measurement method for pass-by noise, total effective roughness, transfer functions and track spatial decay. *Journal of Sound and Vibration*. 2006; 293: 1007-28.
7. Jones CJC, Thompson DJ, Diehl RJ. The use of decay rates to analyse the performance of railway track in rolling noise generation. *Journal of sound and vibration*. 2006; 293: 485-95.
8. ISO 10846-2: 2008. Acoustics and vibration – laboratory measurement of vibro-acoustic transfer properties of resilient elements – part 2: direct method for determination of the dynamic stiffness of resilient supports for

translatory motion.
9. ISO 10846-3: 2002. Acoustics and vibration – laboratory measurement of vibro-acoustic transfer properties of resilient elements – part 3: indirect method for determination of the dynamic stiffness of resilient supports for translatory motion.
10. Thompson DJ, Verheij JW. The dynamic behaviour of rail fasteners at high frequencies. *Applied Acoustics*. 1997; 52: 1-17.
11. Thompson DJ, Van Vliet WJ, Verheij JW. Developments of the indirect method for measuring the high frequency dynamic stiffness of resilient elements. *Journal of Sound and Vibration*. 1998; 213: 169-88.
12. Thompson DJ, Jones CJC, Wu TX, de France A. The influence of the non-linear stiffness behaviour of rail pads on the track component of rolling noise. *Proceedings of the Institution of Mechanical Engineers, Part F: Journal of rail and rapid transit*. 1999; 213: 233-41.
13. Squicciarini G, Thompson DJ, Toward MGR, Cottrell RA. The effect of temperature on railway rolling noise. *Proceedings of the Institution of Mechanical Engineers, Part F: Journal of Rail and Rapid Transit*. 2015: 0954409715614337.
14. Fenander Å. Frequency dependent stiffness and damping of railpads. *Proceedings of the Institution of Mechanical Engineers, Part F: Journal of rail and rapid transit*. 1997; 211: 51-62.
15. Wei K, Wang P, Yang F, Xiao JH. The effect of the frequency-dependent stiffness of rail pad on the environment vibrations induced by subway train running in tunnel. *Proceedings of the Institution of Mechanical Engineers, Part F: Journal of Rail and Rapid Transit*. 2014: 0954409714558438.
16. EN 15461: 2008. Railway applications – noise emissions, characterization of the dynamic properties of track sections for pass by noise measurements.
17. Li WX, Jiang JD, Dwight R, Schulten C. An investigation of a method for track decay rate measurement using train pass-bys. *Proceedings of ACOUSTICS 2011*. Gold Coast, Australia.
18. Dittrich MG, Létourneaux F, Dupuis H. Background for a new standard on pass-by measurement of combined roughness, track decay rate and vibroacoustic transfer functions. *Noise and Vibration Mitigation for Rail Transportation Systems*: Springer, 2015, p. 197-204.
19. Grassie SL. Rail irregularities, corrugation and acoustic roughness: characteristics, significance and effects of reprofiling. *Proceedings of the Institution of Mechanical Engineers, Part F: Journal of Rail and Rapid Transit*. 2012: 0954409712443492.
20. Zhi SD, Li JY, Zarembski AM. Predictive modeling of the rail grinding process using a distributed cutting grain approach. *Proceedings of the Institution of Mechanical Engineers, Part F: Journal of Rail and Rapid Transit*. 2015: 0954409715605139.
21. European Standard EN 15610:2009 C. Railway applications – noise emission – rail roughness measurement related to rolling noise generation. Brussels, Belgium2009.
22. Grassie SL. Short wavelength rail corrugation: field trials and measuring technology. *Wear*. 1996; 191: 149-60.
23. ISO 3095:2013. Railway applications. Acoustics. Measurement of noise emitted by railbound vehicles. .
24. Thompson DJ. On the relationship between wheel and rail surface roughness and rolling noise. *Journal of Sound and Vibration*. 1996; 193: 149-60.
25. Remington PJ. Wheel/rail noise—Part IV: Rolling noise. *Journal of Sound and Vibration*. 1976; 46: 419-36.
26. Remington P, Webb J. Estimation of wheel/rail interaction forces in the contact area due to roughness. *Journal of Sound and Vibration*. 1996; 193: 83-102.
27. Thompson D. The influence of the contact zone on the excitation of wheel/rail noise. *Journal of Sound and Vibration*. 2003; 267: 523-35.
28. Dittrich MG, Janssens MHA. Improved measurement methods for railway rolling noise. *Journal of Sound and Vibration*. 2000; 231: 595-609.
29. Wu TX, Thompson DJ. The influence of random sleeper spacing and ballast stiffness on the vibration behaviour of railway track. *Acta Acustica united with Acustica*. 2000; 86: 313-21.
30. Wu TX, Thompson DJ. A double Timoshenko beam model for vertical vibration analysis of railway track at high frequencies. *Journal of Sound and Vibration*. 1999; 224: 329-48.
31. Nilsson CM, Jones CJC, Thompson DJ, Ryue J. A waveguide finite element and boundary element approach to calculating the sound radiated by railway and tram rails. *Journal of Sound and Vibration*. 2009; 321: 813-36.
32. Ryue J, Thompson DJ, White PR, Thompson DR. Decay rates of propagating waves in railway tracks at high frequencies. *Journal of Sound and Vibration*. 2009; 320: 955-76.
33. Li Q, Wu DJ. Analysis of the dominant vibration frequencies of rail bridges for structure-borne noise using a power flow method. *Journal of Sound and Vibration*. 2013; 332: 4153-63.
34. Li Q, Li WQ, Wu DJ, Song XD. A combined power flow and infinite element approach to the simulation of medium-frequency noise radiated from bridges and rails. *Journal of Sound and Vibration*. 2016; 365: 134-56.

35. Nilsson CM, Jones CJC. Theory manual for WANDS 2.1 wave number domain FE-BE software for structures and fluids. 2007.
36. Wu TX, Thompson DJ. Vibration analysis of railway track with multiple wheels on the rail. *Journal of Sound and Vibration*. 2001; 239: 69-97.

**Table 1 Track parameters for simulations in this study**

| Track | Stiff | Medium | Soft | Very soft | Estimated (unloaded) |
|---|---|---|---|---|---|
| Rail pad stiffness per fastener | 600 MN/m | 300 MN/m | 120 MN/m | 60 MN/m | 600 MN/m |
| Loss factor of rail pad | 0.05 | 0.1 | 0.15 | 0.20 | 0.25 |
| Ballast stiffness per fastener | 48 MN/m | 90 MN/m | 120 MN/m | 360 MN/m | 42 MN/m |
| Loss factor of Ballast | 2.0 | 1.5 | 1.0 | 0.5 | 1.0 |
| Loss factor of rail | 0.05 | 0.04 | 0.03 | 0.02 | 0.01 |

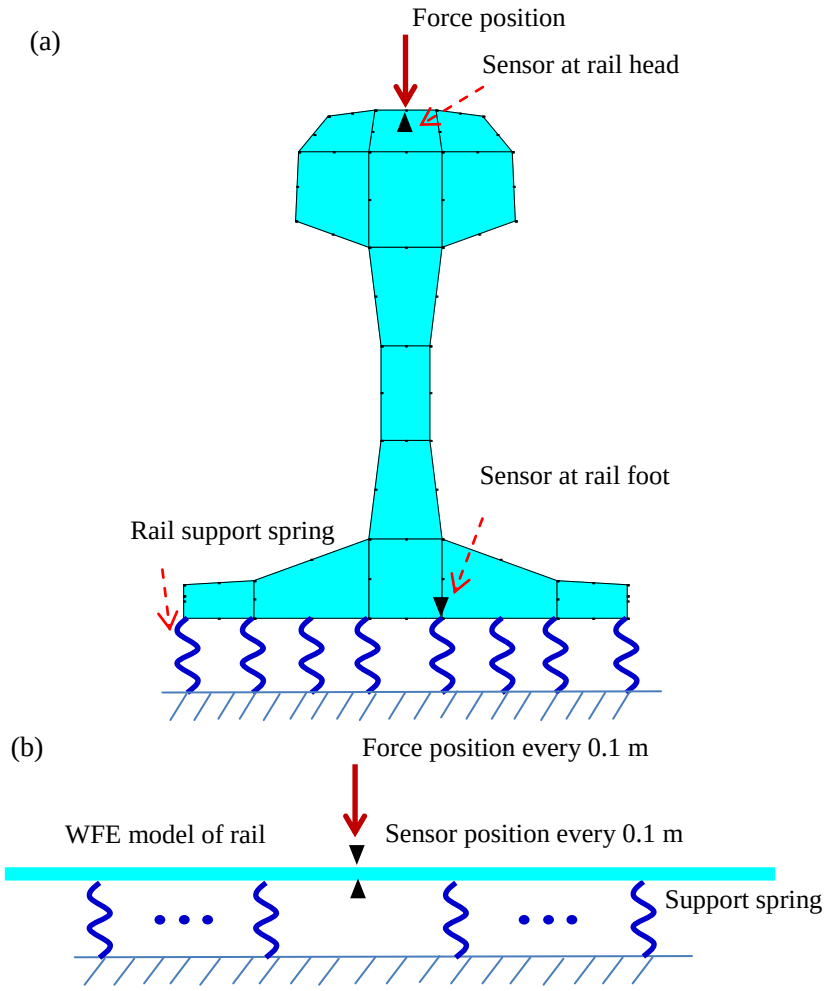


Figure 1. Model of the track: (a) WFE mesh of the rail and springs distributed across rail foot; (c) rail on discrete springs in the longitudinal direction

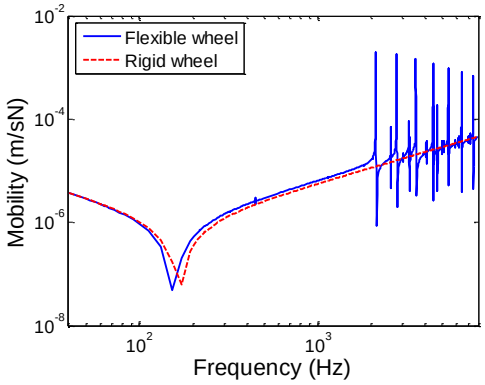


Figure 2. Magnitude of the sum of the mobilities of the wheel and the contact spring in radial direction

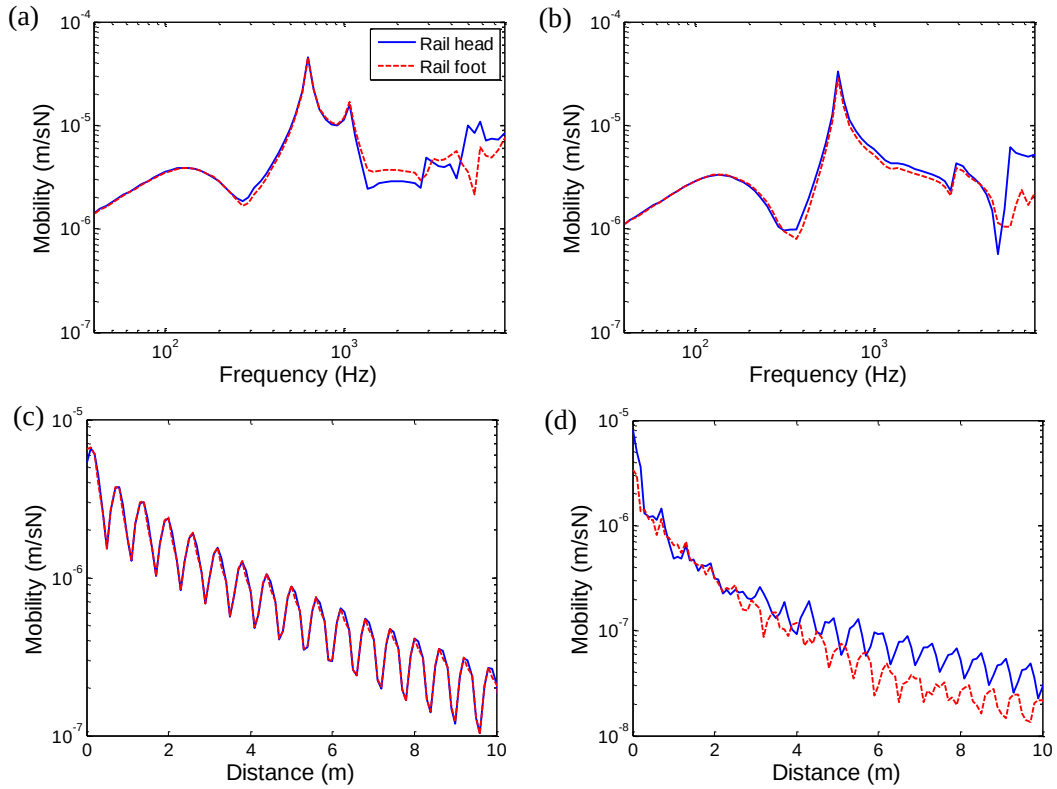


Figure 3. Simulated magnitude of mobilities from the rail on discrete supports (stiff track), excited on rail head at mid-span: (a) driving point mobilities at $x$=0 m; (b) mobilities at $x$=0.3 m; (c) mobilities along the rail at 1250 Hz; (d) mobilities along the rail at 5000 Hz

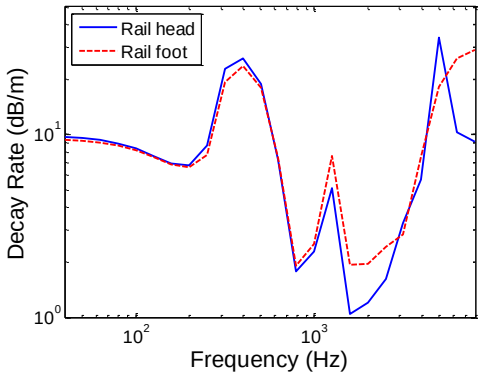


Figure 4. Estimated TDRs from simulated rail head and foot mobilities (stiff track)

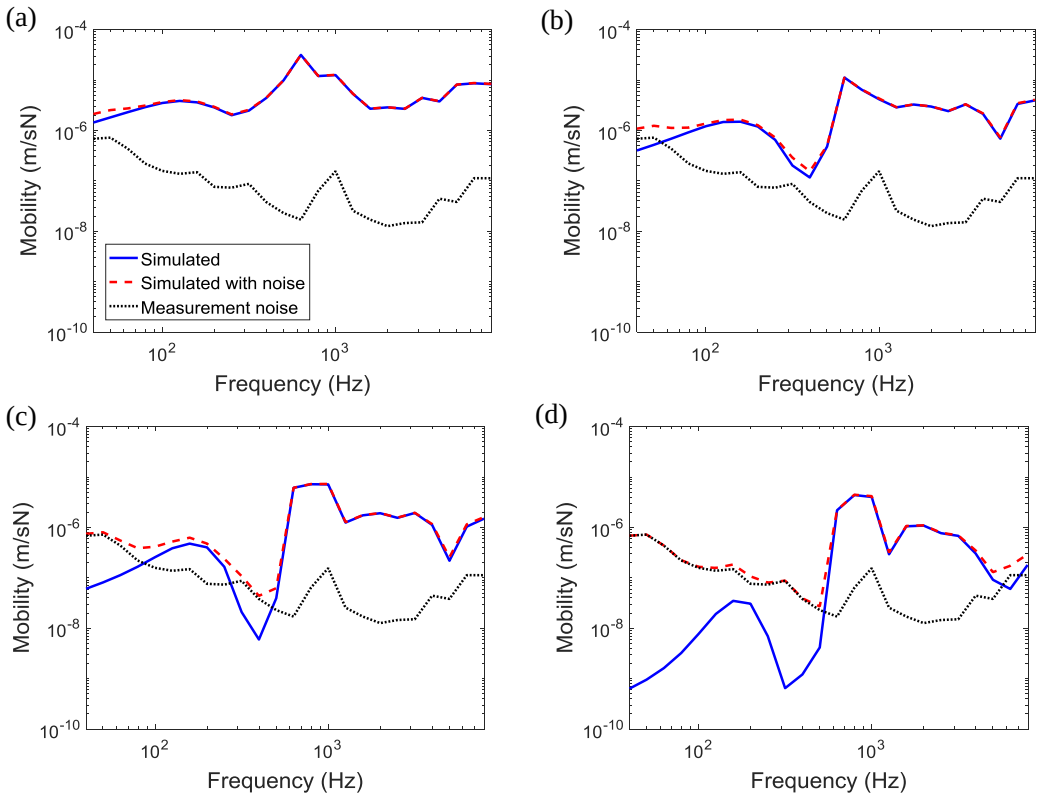


Figure 5. Simulated magnitude of mobilities at the rail head due to excitation at the rail head (stiff track): (a) driving point, $x$=0 m; (b) $x$=0.9 m; (c) $x$=2.4 m; and (d) $x$=6.0 m

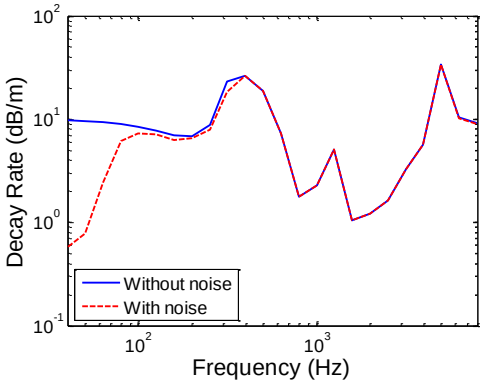


Figure 6. Estimated TDRs from simulated rail head mobilities with and without measurement noise (stiff track)

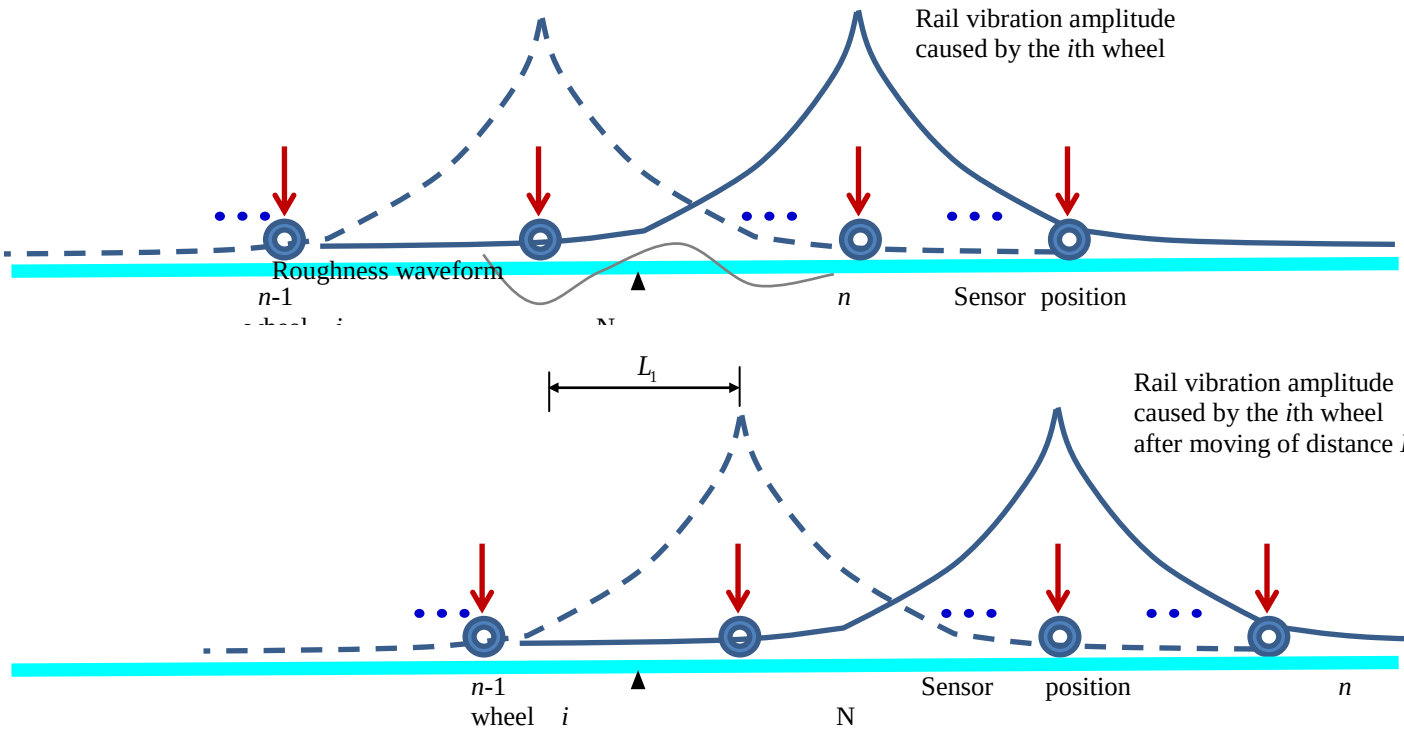


Figure 7. Illustration of rail vibration at fixed position produced by the moving wheels

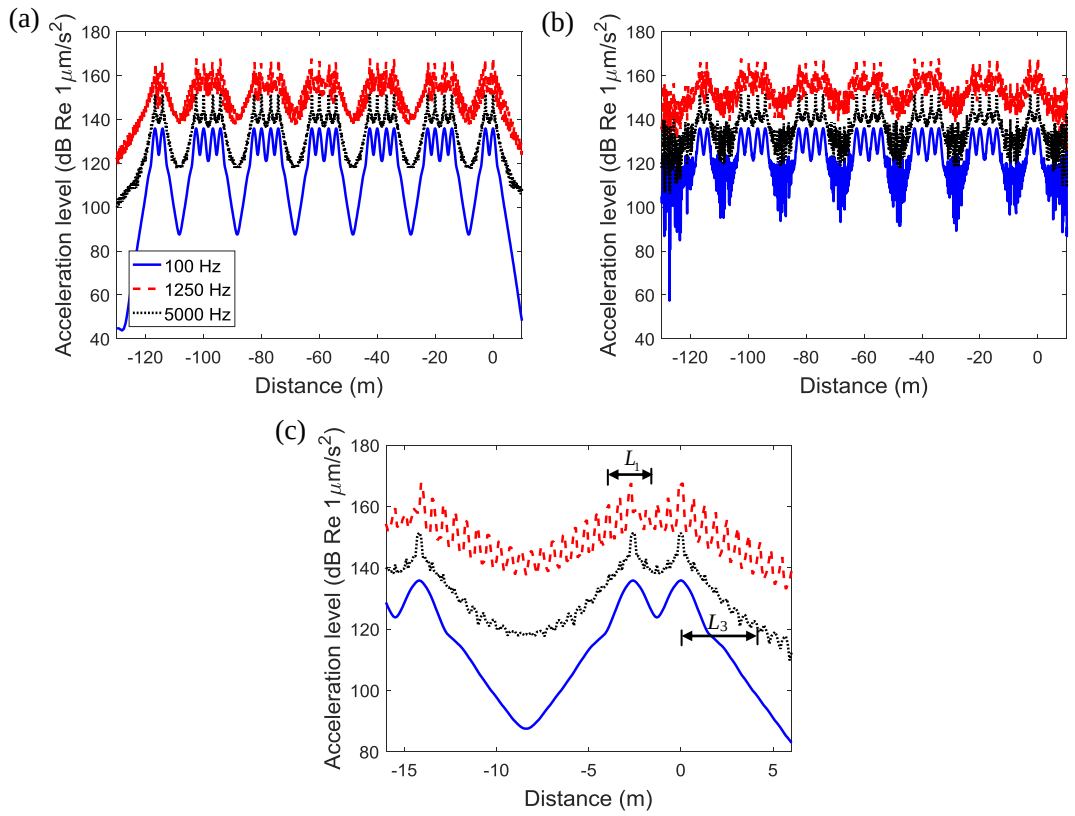


Figure 8. Simulated instantaneous acceleration levels at rail foot (stiff track): (a) no measurement error; (b) with Gaussian noise with standard deviation equal to 10% of maximum acceleration amplitude in each frequency band; (c) zoom of (a)

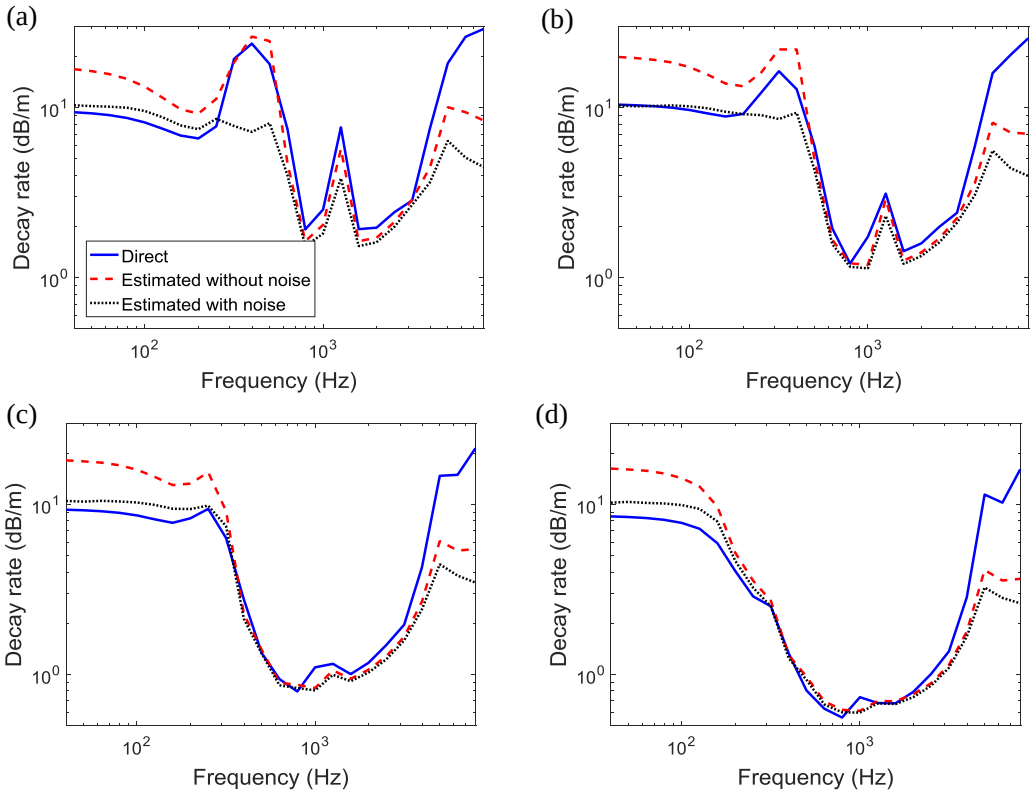


Figure 9. Estimated TDR from simulated rail foot acceleration using energy iteration method ($L_1$=2.0 m): (a) stiff track; (b) medium track; (c) soft track; and (d) very soft track

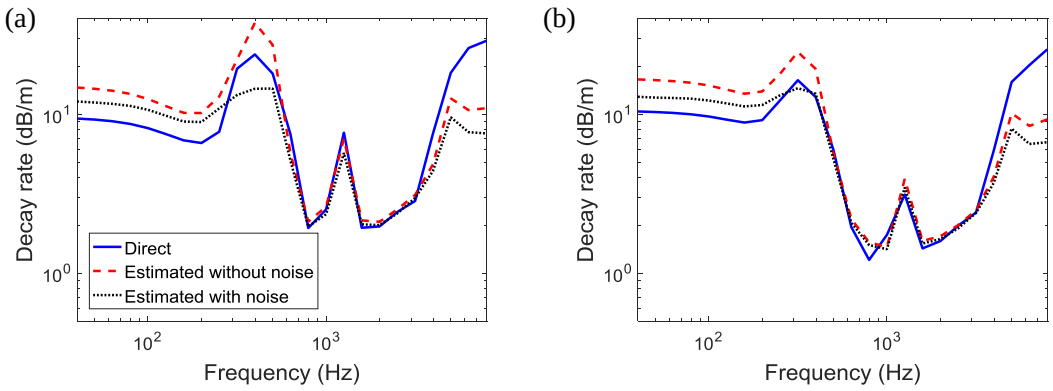


Figure 10. Estimated TDR from simulated rail foot acceleration using energy iteration method ($L_1$=1.0 m): (a) stiff track; (b) medium track

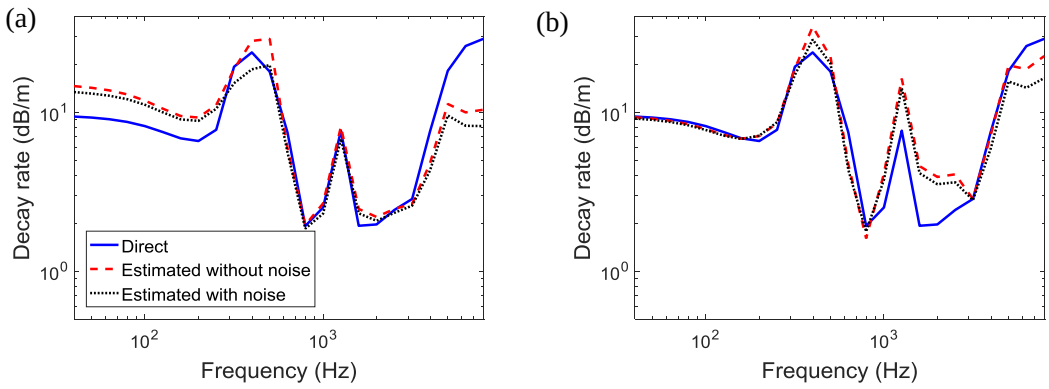


Figure 11. Estimated TDR from simulated rail foot acceleration using slope fitting method (stiff track) with different fitting distance $L_3$: (a) 1.2 m; (b) 0.6 m

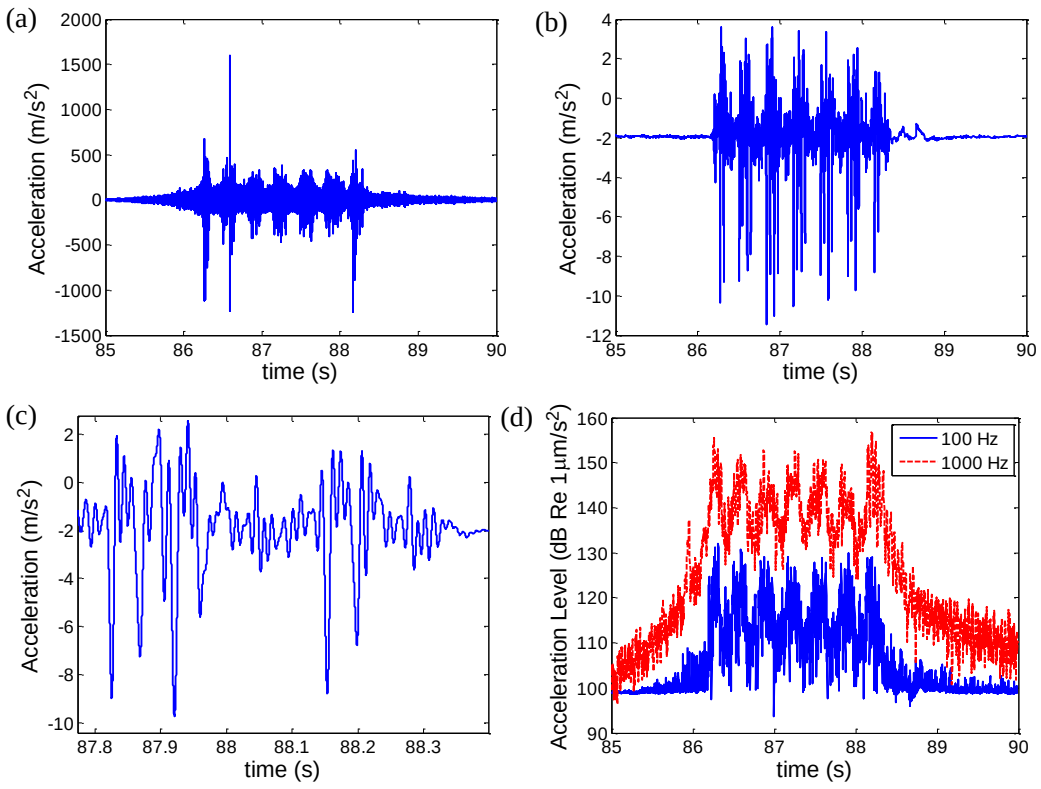


Figure 12. Measured vertical acceleration of rail at train speed 218 km/h: (a) original data; (b) after low–pass filtering with a cut-off of 100 Hz; (c) zoom of (b); and (d) time history of acceleration level

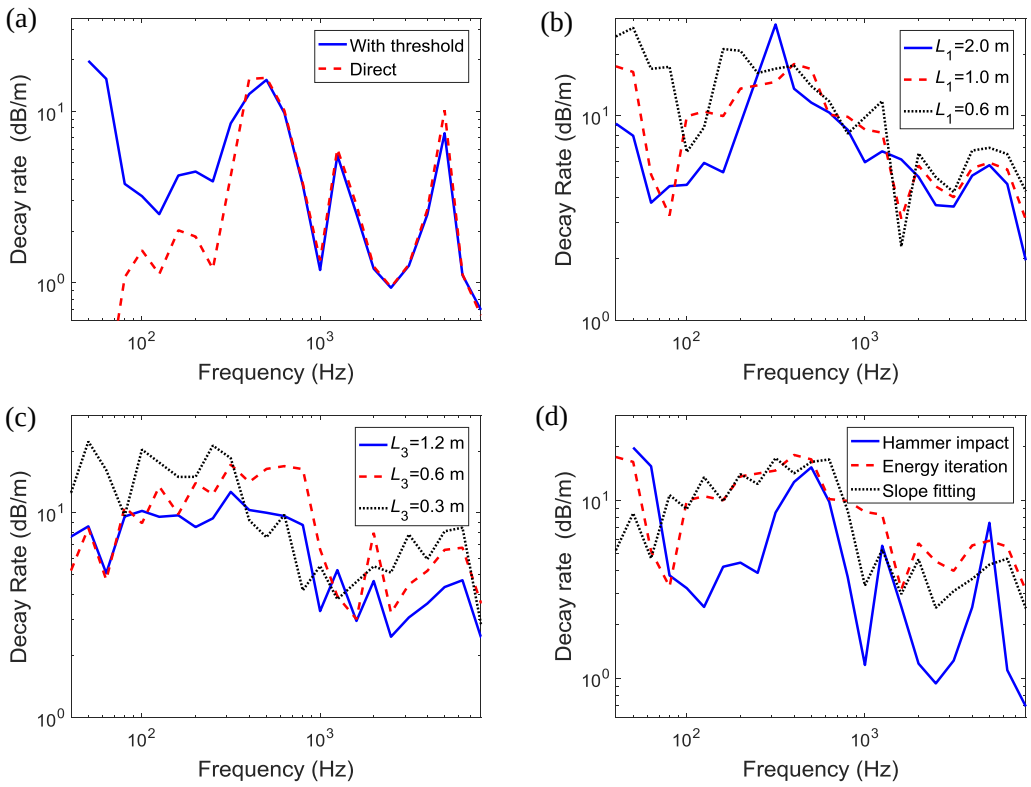


Figure 13. Estimated TDRs from measured rail vibration: (a) hammer impact method; (b) pass-by method, energy iteration; (c) pass-by method, slope fitting; and (d) comparison of different methods

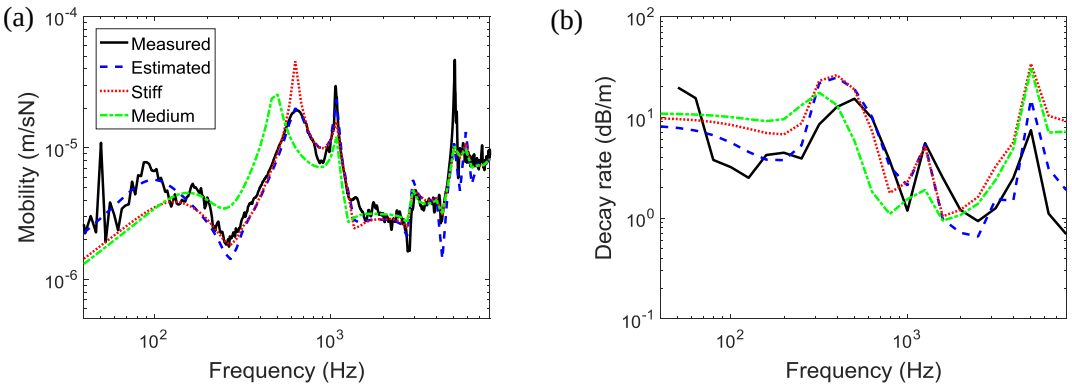


Figure 14. Comparison of measured mobilities and TDRs with simulated results for various tracks: (a) driving point mobilities at rail head; (b) TDRs

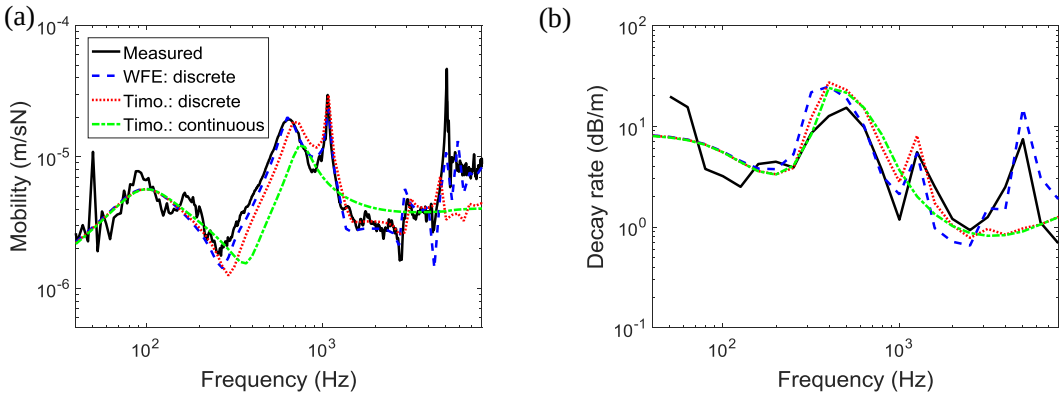


Figure 15. Comparison of measured mobilities and TDRs with simulated results from various track models (estimated track): (a) driving point mobilities at rail head; (b) TDRs

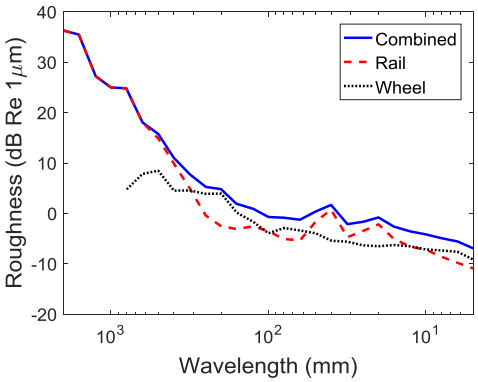


Figure 16. Rail, wheel and combined roughness levels from direct measurements

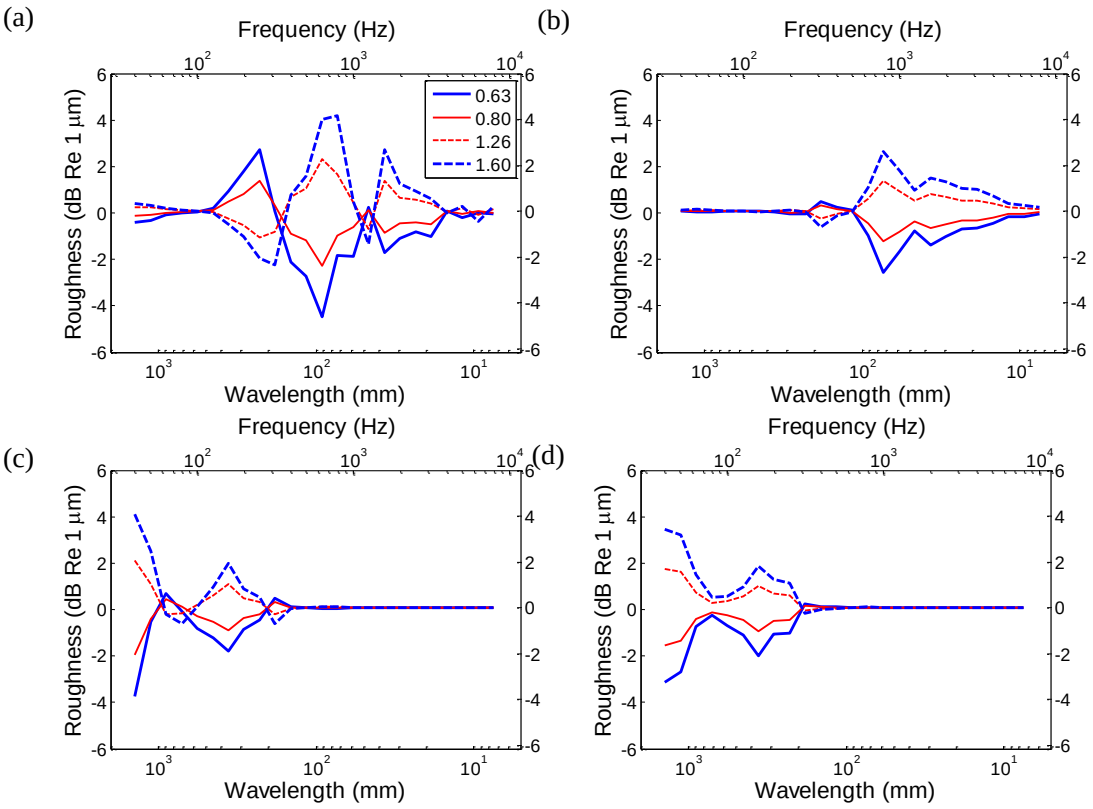


Figure 17. Estimation error of roughness by the full method adopting different changes in the estimated track parameters (215 km/h): (a) pad stiffness; (b) loss factor of pad; (c) ballast stiffness; and (d) loss factor of ballast

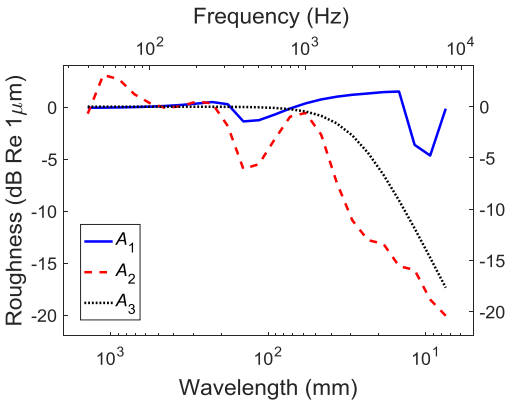


Figure 18. Variation of $A_1$, $A_2$ and $A_3$ with frequency and wavelength (215 km/h)

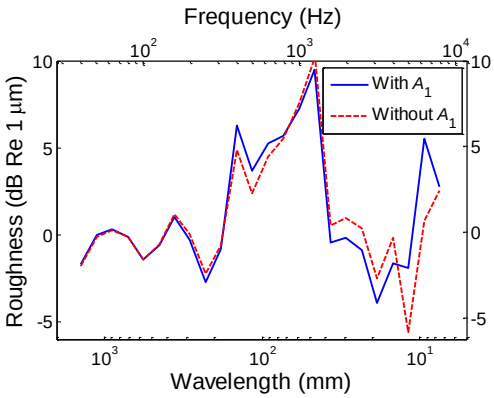


Figure 19. Estimation error of roughness by the simplified pass-by method (215 km/h)

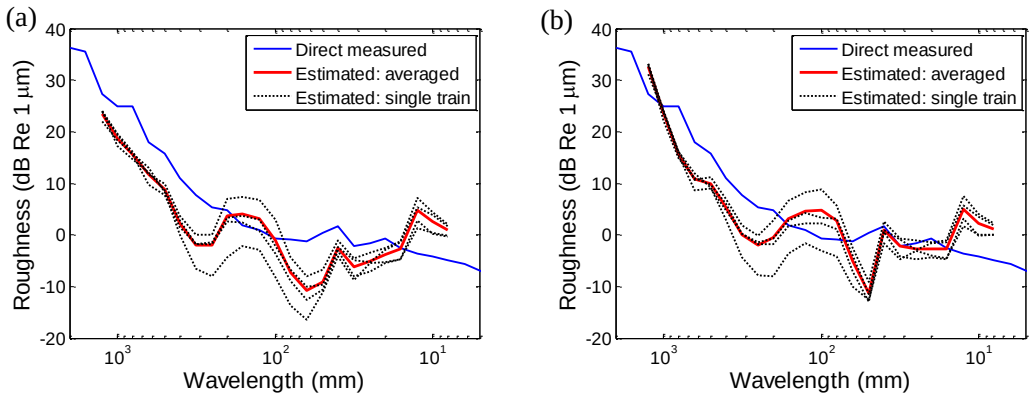


Figure 20. Estimated roughness by the full method with different track parameters: (a) estimated track; and (b) pad stiffness and ballast stiffness of the estimated track increased by a factor of 3.

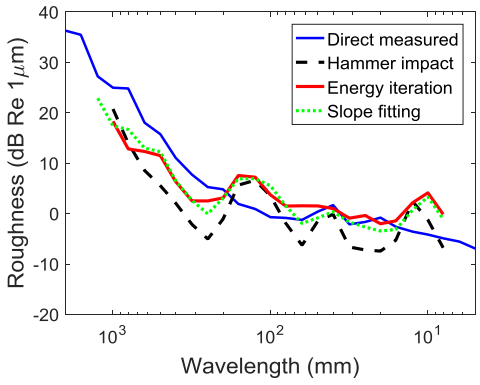


Figure 21. Estimated roughness by the simplified method with different measured TDRs from hammer impact, energy iteration and slope fitting methods